Unraveling the Effect of Alkali Cation on Fe Single Atom Catalyst with High Coordination Number

Yecheng Li[§a], Songjie Meng[§b], Zihong Wang[c], Hehe Zhang[d], Xin Zhao[c], Qingshun Nian[c], Digen Ruan[c], Lianfeng Zou[*d], Zhansheng Lu[*b,e], and Xiaodi Ren[*a,c]

[a] Y. Li, Prof. X. Ren

Hefei National Laboratory for Physical Sciences at the Microscale, CAS Key Laboratory of Materials for Energy Conversion, University of Science and Technology of China, Anhui 230026, China.

[b] S. Meng, Prof. Z. Lu

School of Physics, Henan Normal University, Xinxiang 453007, China.

[c] Z. Wang, X. Zhao, Q. Nian, D. Ruan, Prof. X. Ren

School of Chemistry and Materials Science, University of Science and Technology of China, Anhui 230026, China.

[d] H. Zhang, Prof. L. Zou

Clean Nano Energy Center, State Key Laboratory of Metastable Material Science and Technology, Yanshan University, Qinhuangdao, 066004 China.

[e] Prof. Z. Lu

College of Mathematics and Physics, Beijing University of Chemical Technology, Beijing 100029, China.

*Corresponding author

E-mail address: zoulf@ysu.edu.cn, zslu@buct.eud.cn, xdren@ustc.edu.cn

Figures and Tables

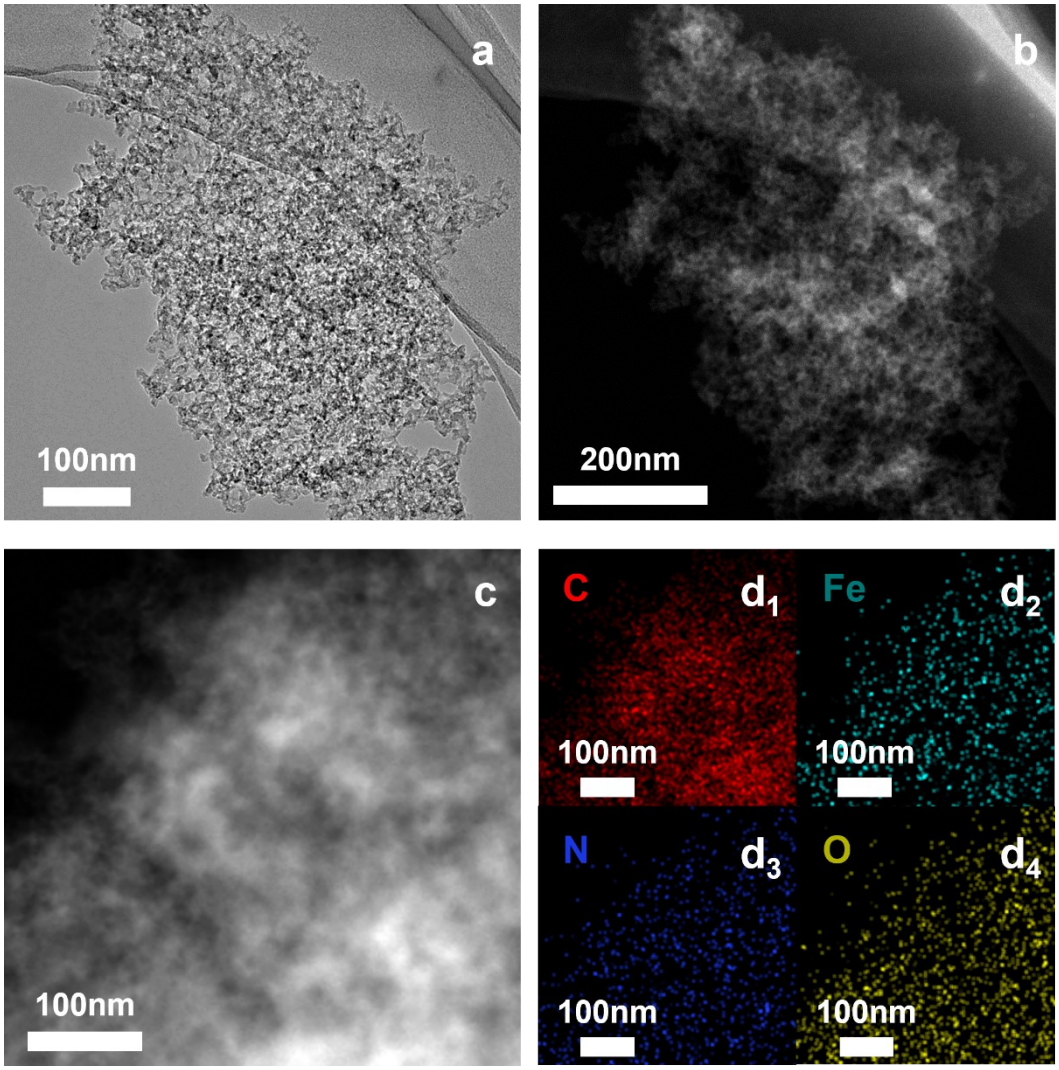

Figure S1. (a) The TEM image of FeN_6. (b) – (c) HADDF-STEM image of of FeN_6. (d) EDS mapping image of FeN_6, corresponding to C, Fe, N, and O element.

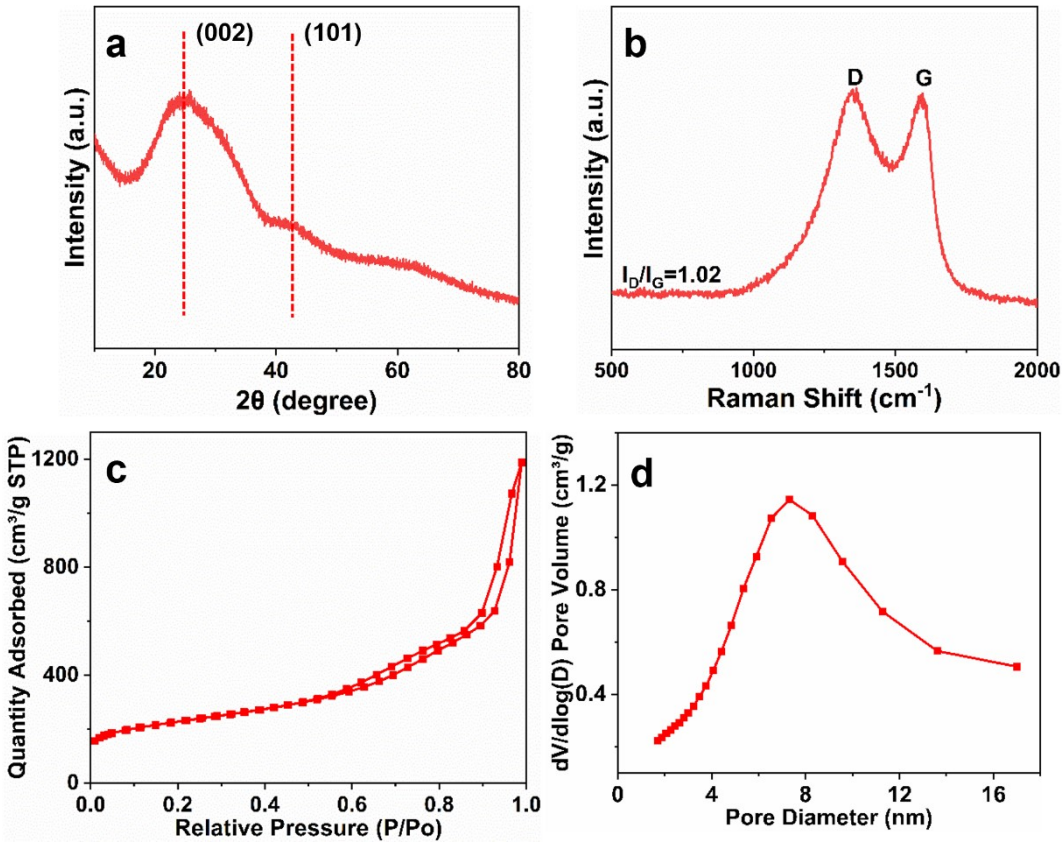

Figure S2. (a) The XRD image of FeN_6. (b) The Raman image of FeN_6. (c) The N_2 adsorption/desorption isotherms of FeN_6. (d) The pore size distribution of FeN_6.

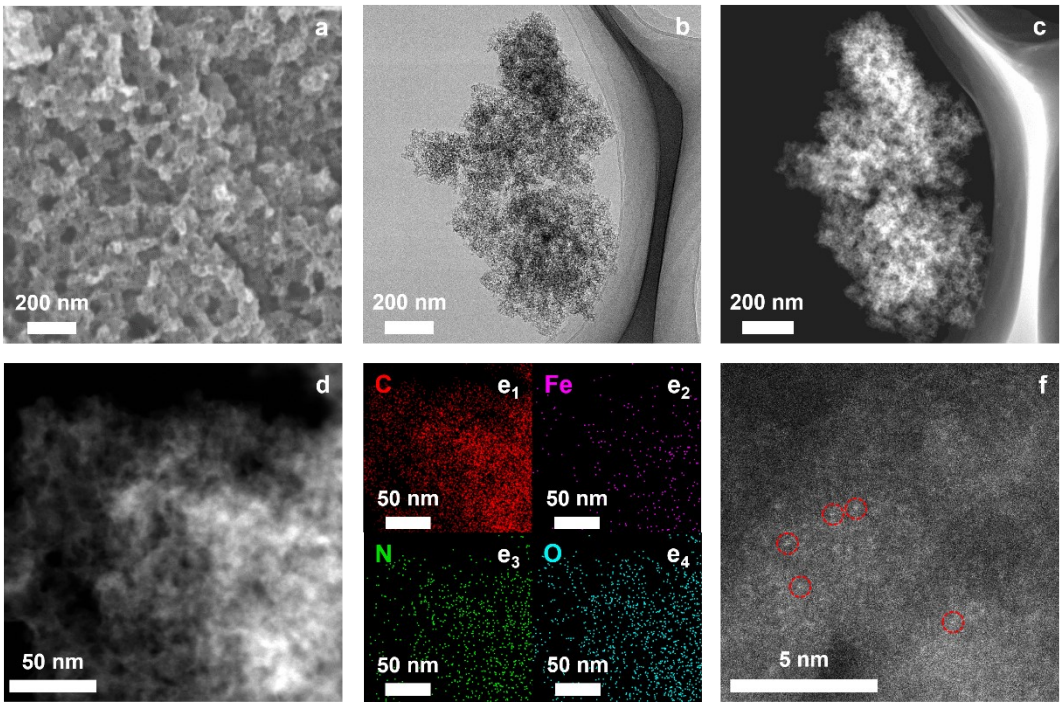

Figure S3. The morphology of catalyst. (a) SEM image of FeN_5. (b) TEM image of FeN_5. (c) - (d) HADDF-STEM image of FeN_5. (e_1) – (e_4) EDS mapping image of FeN_5, corresponding to C, Fe, N, and O element. (f) AC-HADDF-STEM image of FeN_5 (red circles are the Fe single atom sites).

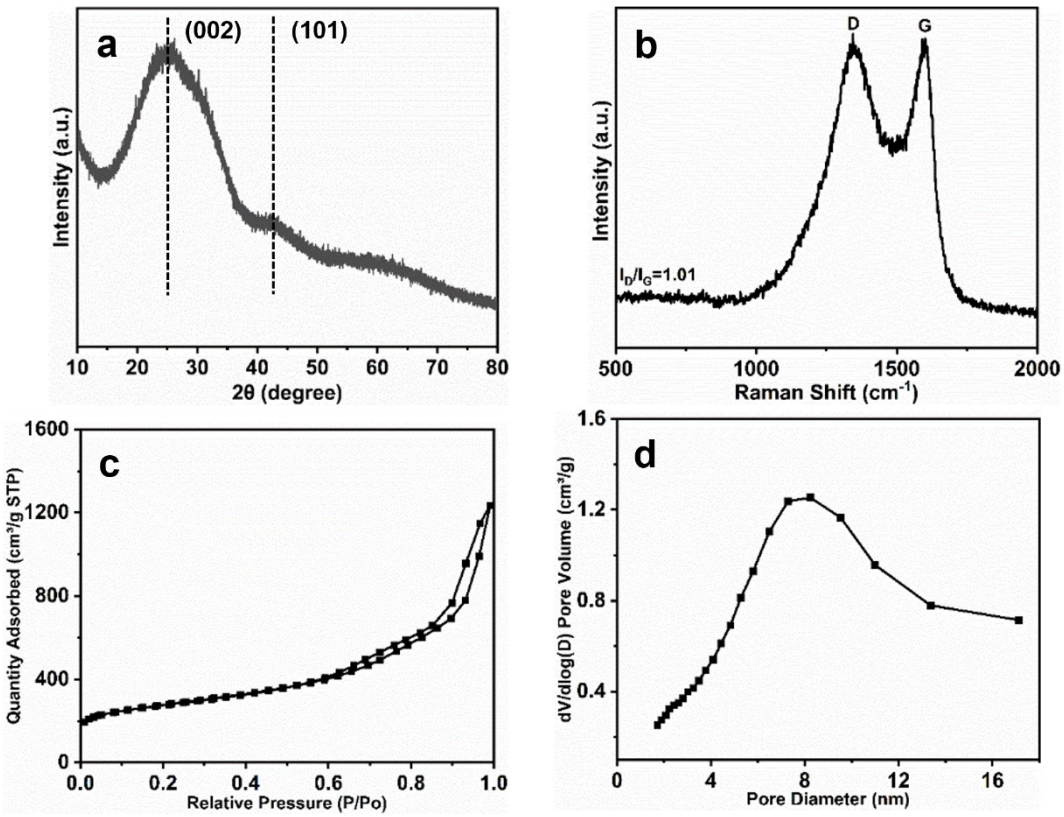

Figure S4. (a) The XRD image of FeN_5. (b) The Raman image of FeN_5. (c) The N_2 adsorption/desorption isotherms of FeN_5. (d) The pore size distribution of FeN_5.

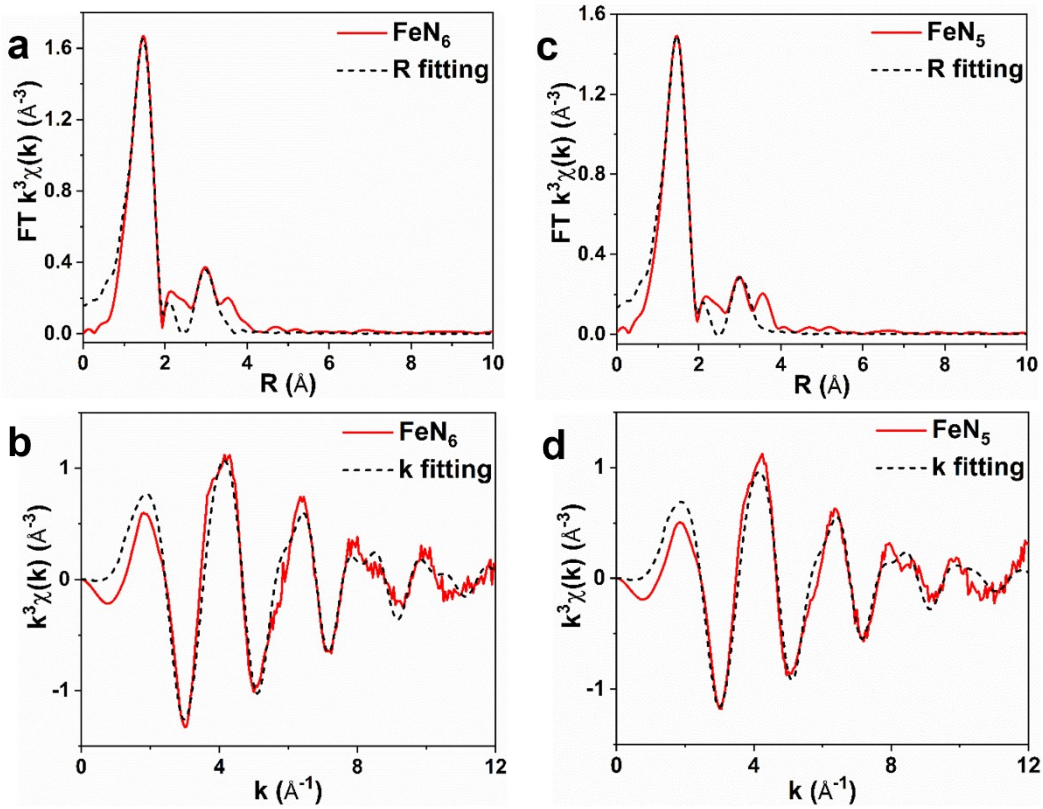

Figure S5. FT-EXAFS fitting curves of Fe k-edge FeN_5 and FeN_6, related to Figure 2. (a) - (b) FT-EXAFS fitting curves at R spaces. (c) - (d) FT-EXAFS fitting curves at k spaces.

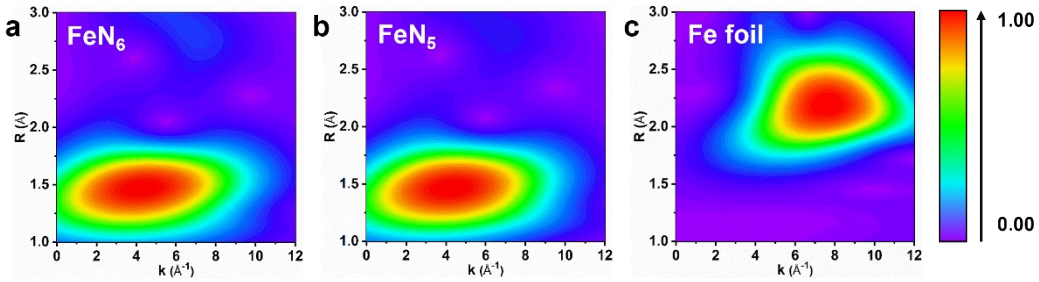

Figure S6. The WT-EXAFS spectra of (a) FeN_6, (b) FeN_5 and (c) Fe foil.

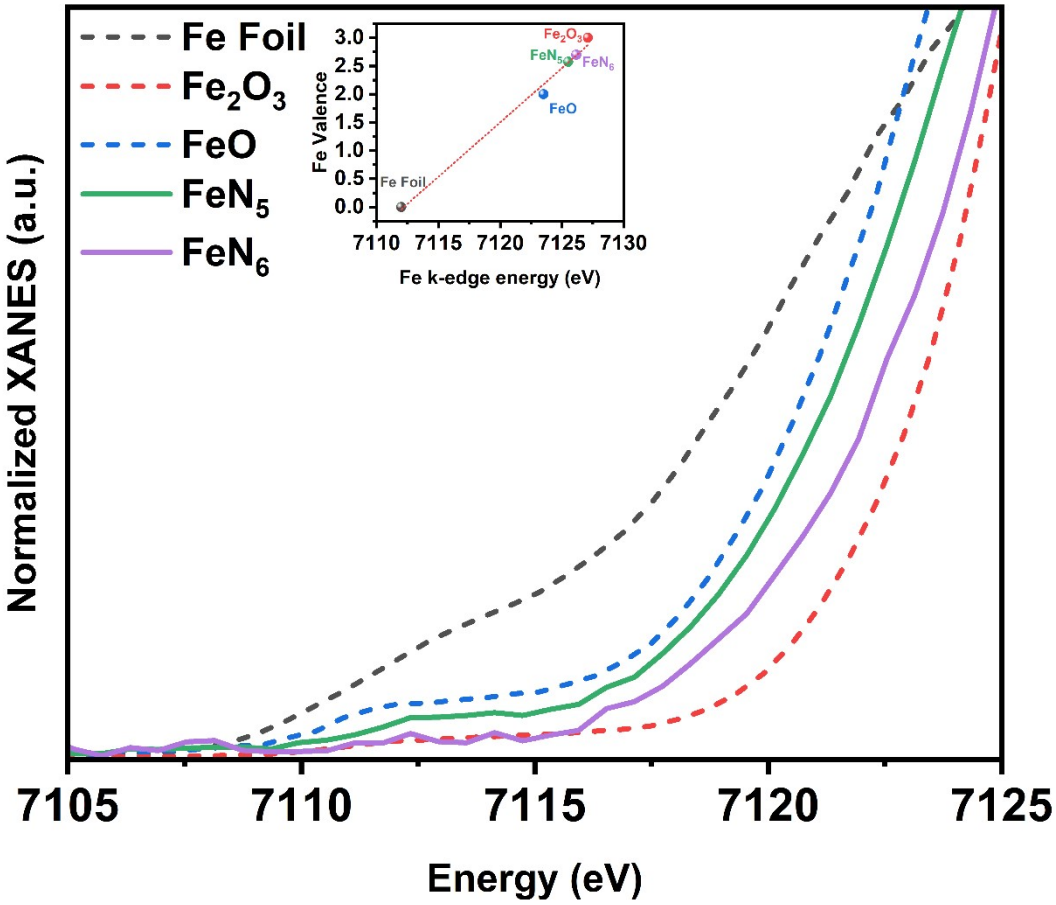

Figure S7. Fe K-edge XANES spectra and Fe valence state.

the valence state of Fe in FeN_5 and FeN_6 can be calculated to be 2.58 and 2.70 respectively. This result is consistent with our XPS analysis (Table S3), which shows that the valence state of Fe in FeN_x is between +2 and +3, and the valence state of Fe in FeN_6 is higher than FeN_5.

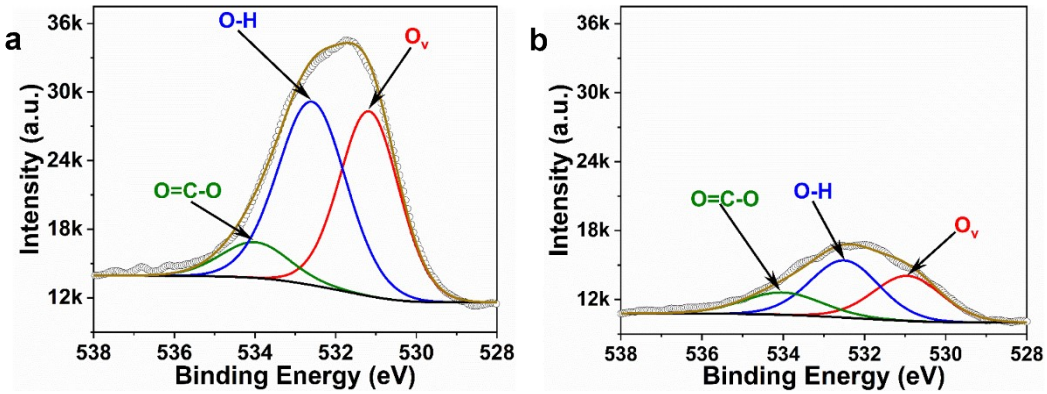

Figure S8. (a) The O spectrum of FeN_6. (b) The O spectrum of FeN_5.

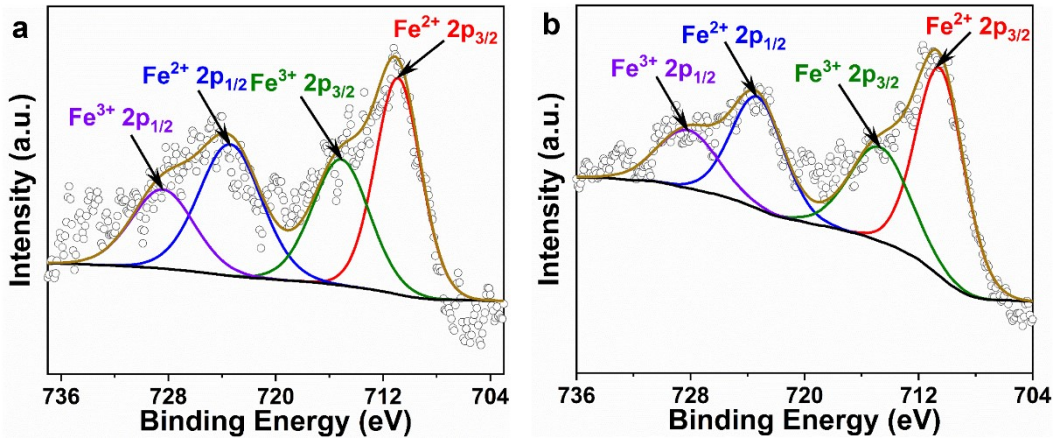

Figure S9. (a) The Fe spectrum of FeN_6. (d) The Fe spectrum of FeN_5.

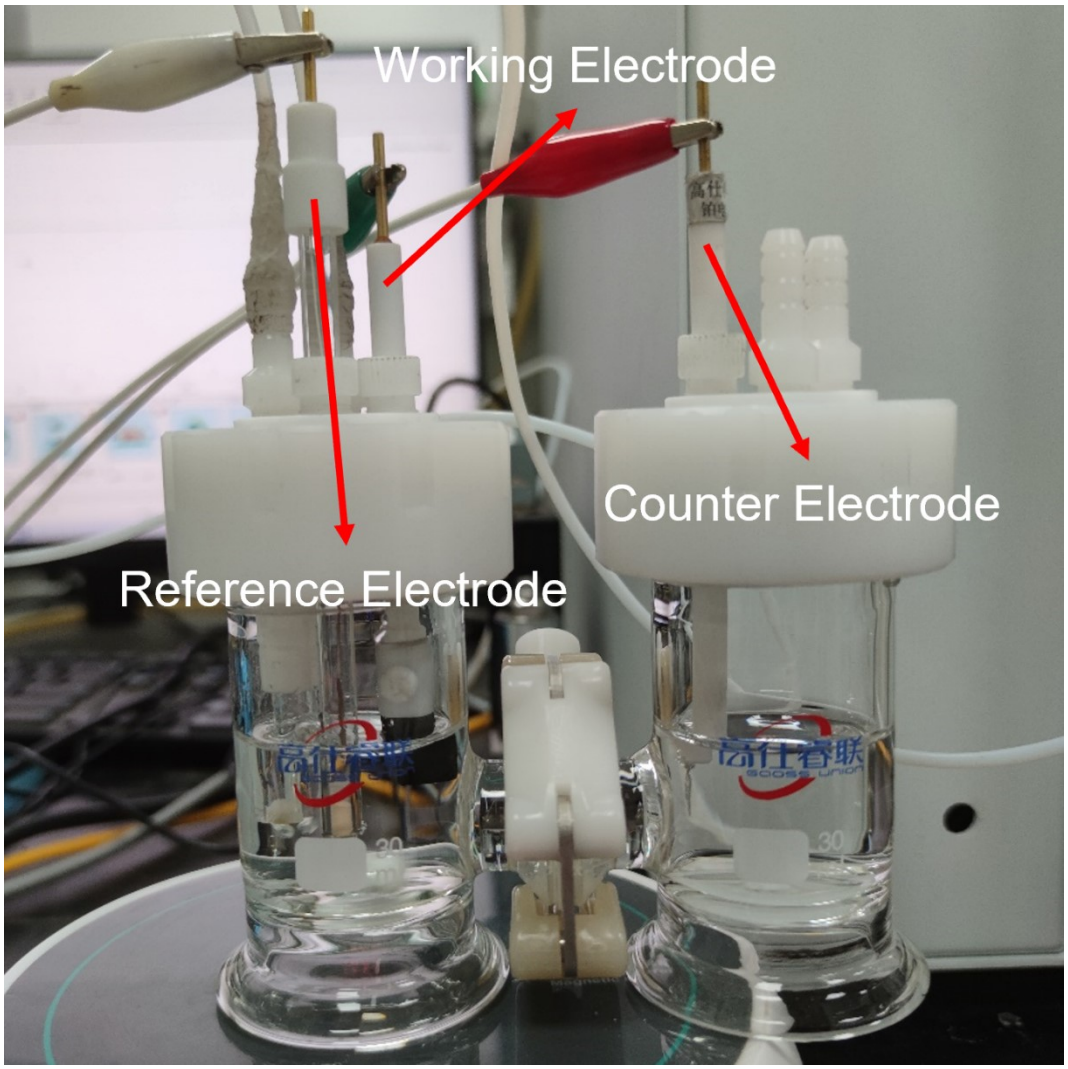

Figure S10. The H-type three-electrode system cell for electrochemical measurement.

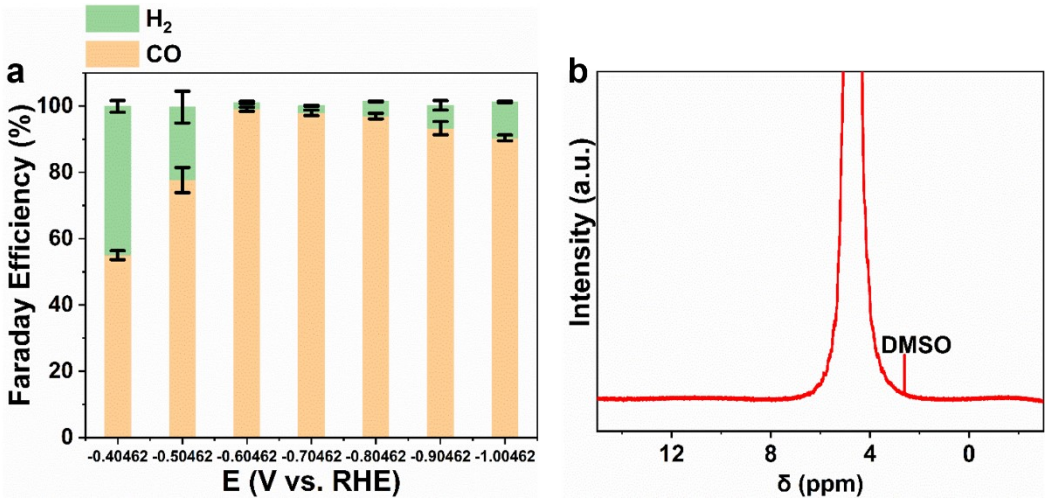

Figure S11. The selectivity of FeN_6. (a) The total FE in 0.1 M $NaHCO_3$. (b) The H NMR spectroscopy in 0.1 M $NaHCO_3$ (After all selectivity tests).

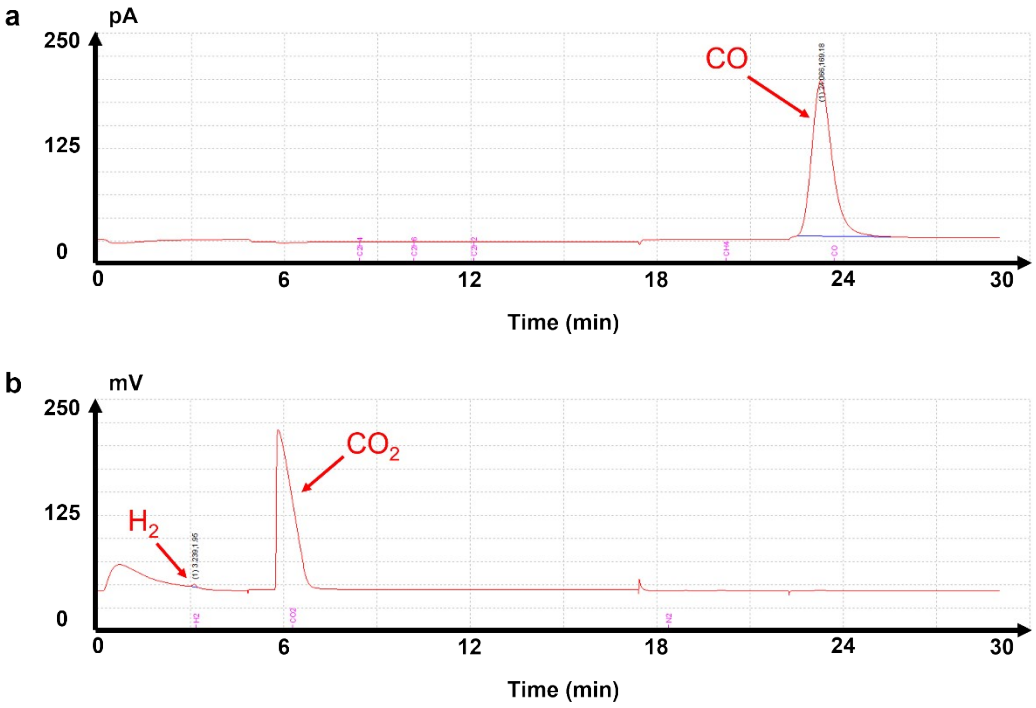

Figure S12. The GC of FeN_6 in CO_2 atmosphere (0.1 M $RbHCO_3$, -0.60 V vs. RHE). (a) The FID curve. (b) The TCD curve.

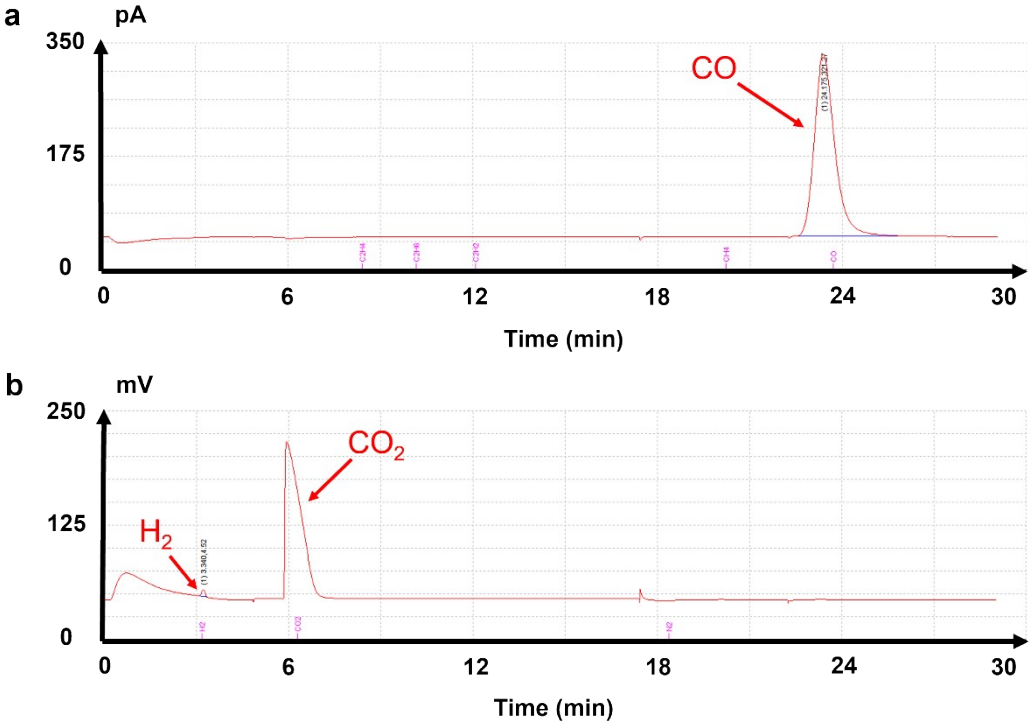

Figure S13. The GC of FeN_5 in CO_2 atmosphere (0.1 M $RbHCO_3$, -0.60 V vs. RHE). (a) The FID curve. (b) The TCD curve.

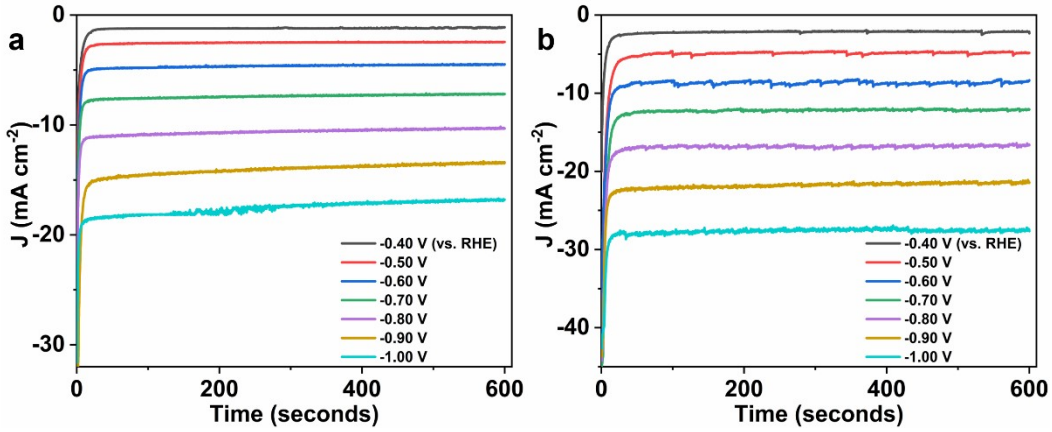

Figure S14. The I-t curves in 0.1 M $RbHCO_3$. (a) The FeN_6 SAC. (b) The FeN_5 SAC.

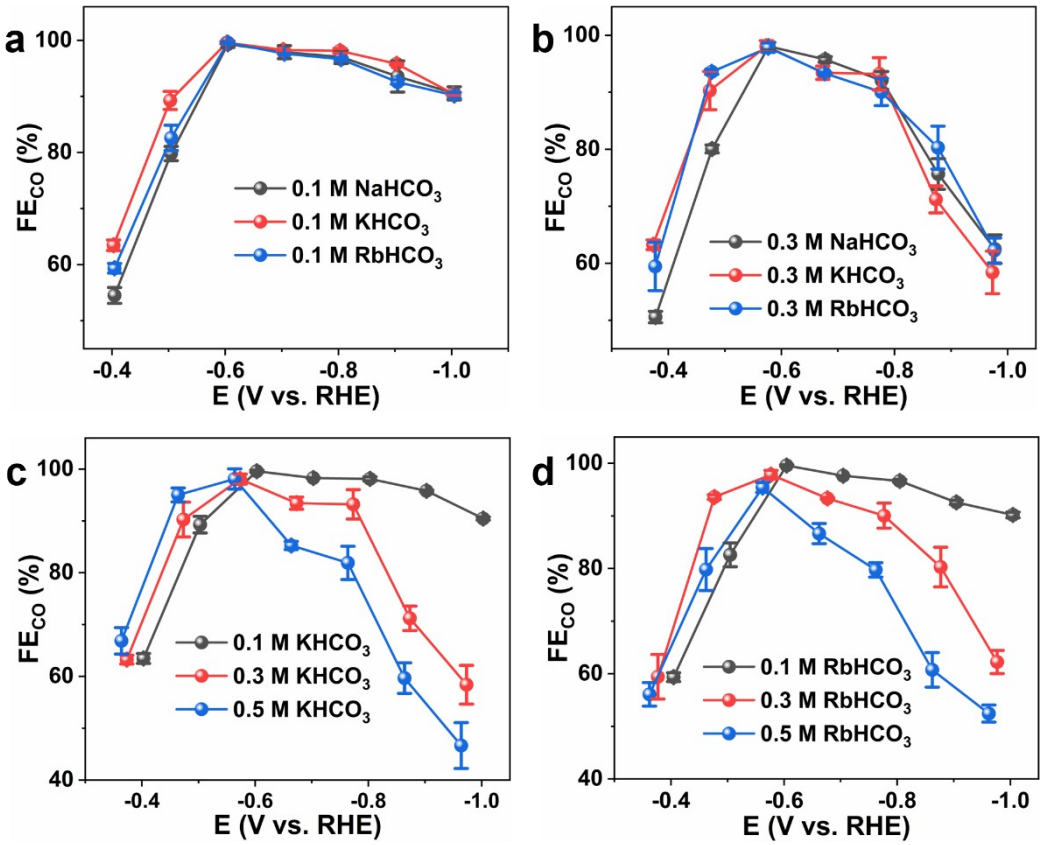

Figure S15. The FE_{CO} of FeN_6 in different electrolyte. (a) 0.1 M and (b) 0.3 M with different cation. (c) $KHCO_3$ and (d) $RbHCO_3$ with different concentration.

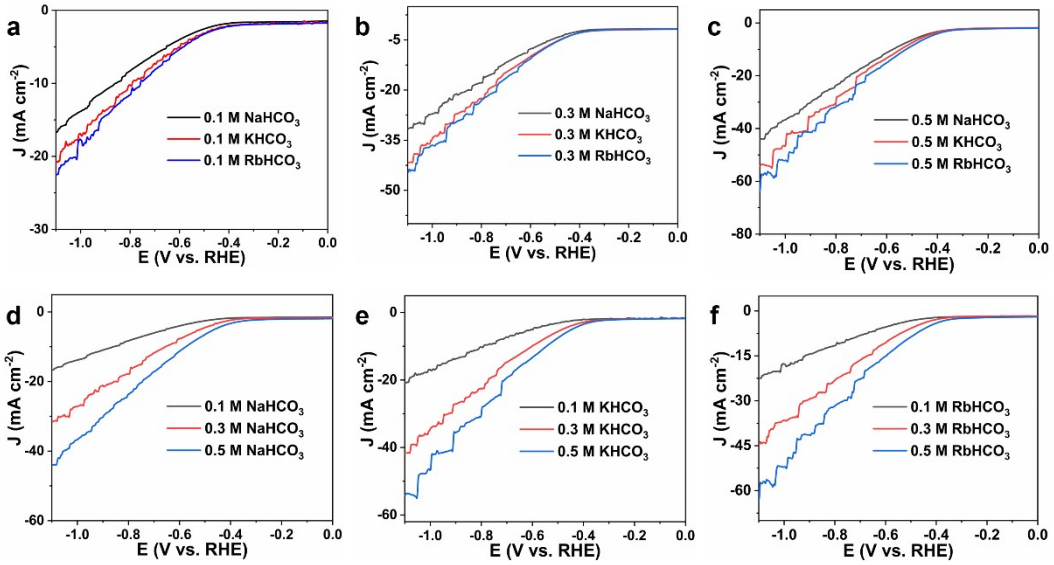

Figure S16. The LSV curves of FeN_6 in different electrolyte. (a) - (c) 0.1 M, 0.3M, and 0.5 M with different cation. (d) – (f) $NaHCO_3$, $KHCO_3$, and $RbHCO_3$ in different concentration respectively.

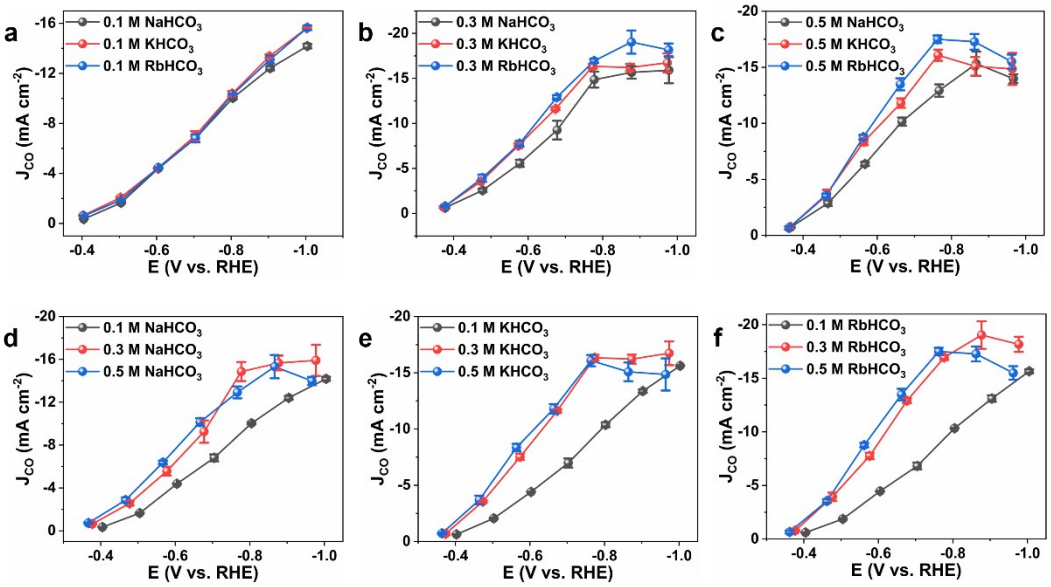

Figure S17. The J_{CO} of FeN_6 in different electrolyte. (a) - (c) 0.1 M, 0.3M, and 0.5 M with different cation. (d) – (f) $NaHCO_3$, $KHCO_3$, and $RbHCO_3$ in different concentration respectively.

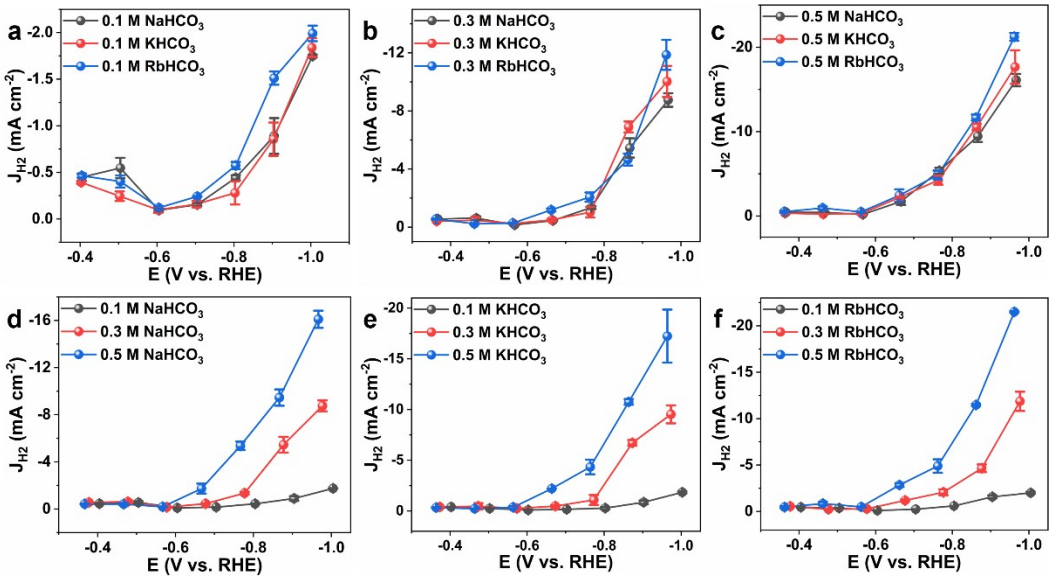

Figure S18. The J_{H2} of FeN_6 in different electrolyte. (a) - (c) 0.1 M, 0.3M, and 0.5 M with different cation. (d) – (f) $NaHCO_3$, $KHCO_3$, and $RbHCO_3$ in different concentration respectively.

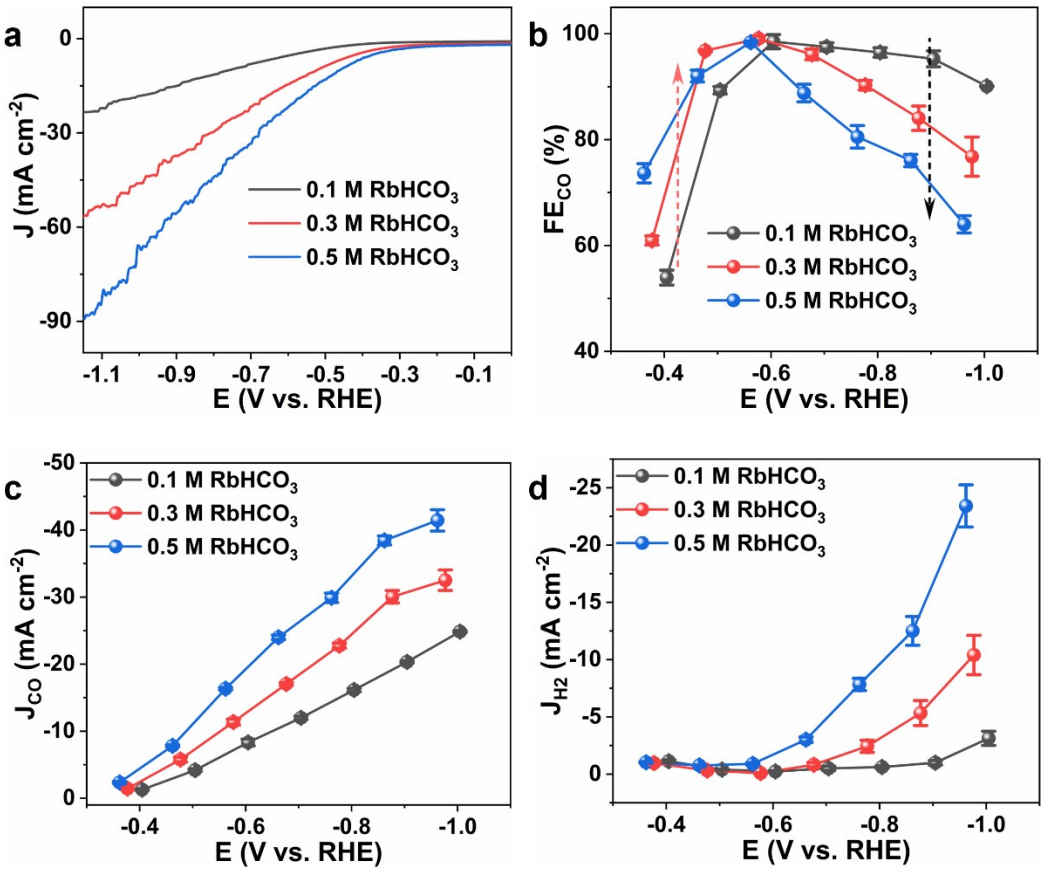

Figure S19. The performance of FeN_5 with different concentration. (a) The LSV curves of FeN_5 in $RbHCO_3$. (b) The FE_{CO} of FeN_5 in $RbHCO_3$. (c) The J_{CO} of FeN_5 in $RbHCO_3$. (d) The J_{H2} of FeN_5 in $RbHCO_3$.

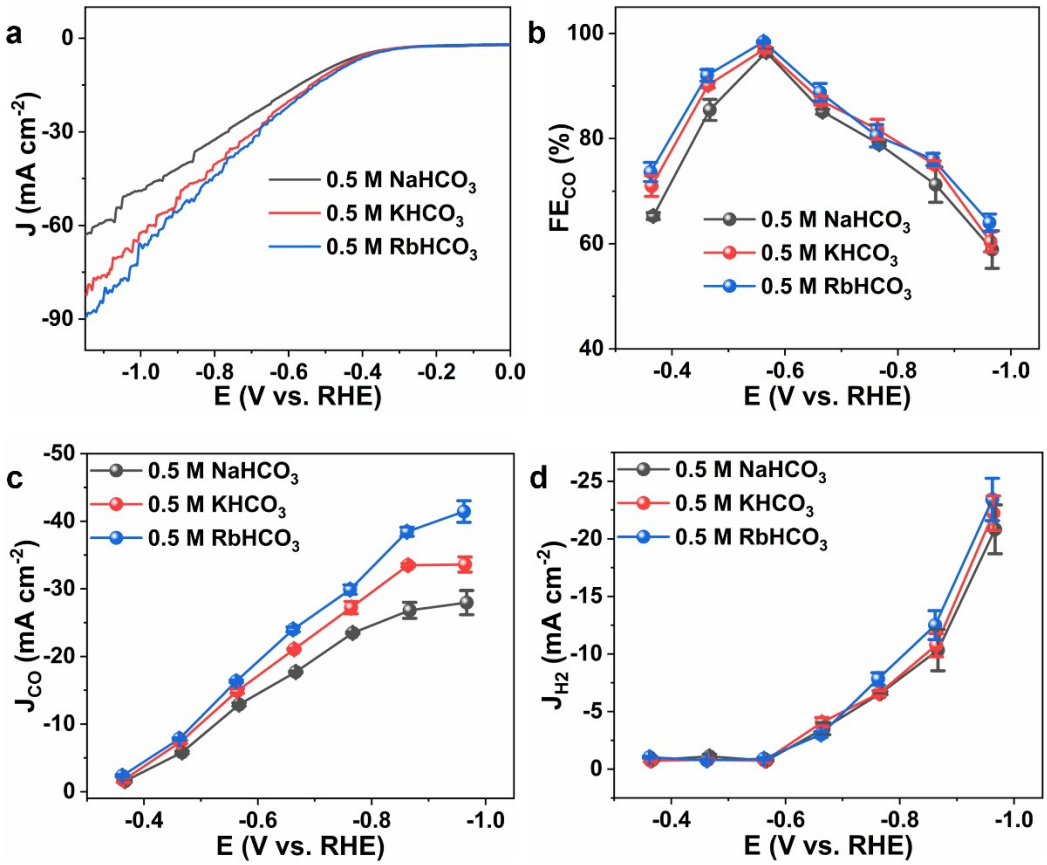

Figure S20. The performance of FeN_5 with different cation. (a) The LSV curves of FeN_5 in 0.5 M. (b) The FE_{CO} of FeN_5 in 0.5 M. (c) The J_{CO} of FeN_5 in 0.5 M. (d) The J_{H2} of FeN_5 in 0.5 M.

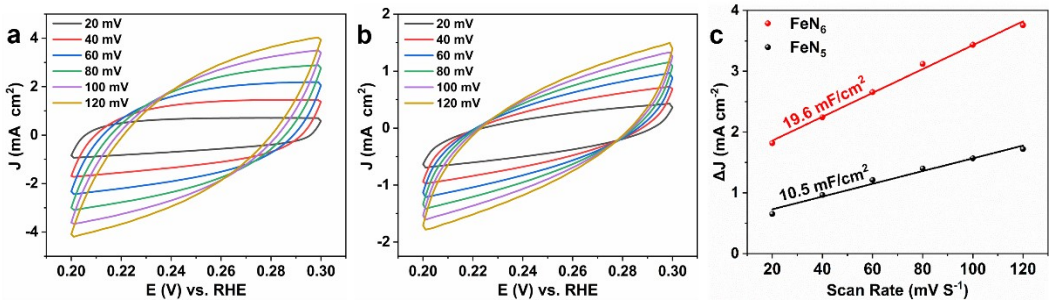

Figure S21. Cyclic voltammetry curves for (a) FeN_6 and (b) FeN_5 with the scan rate from 20mV/s ~ 120mV/s. (c) The C_{dl} for FeN_6 and FeN_5.

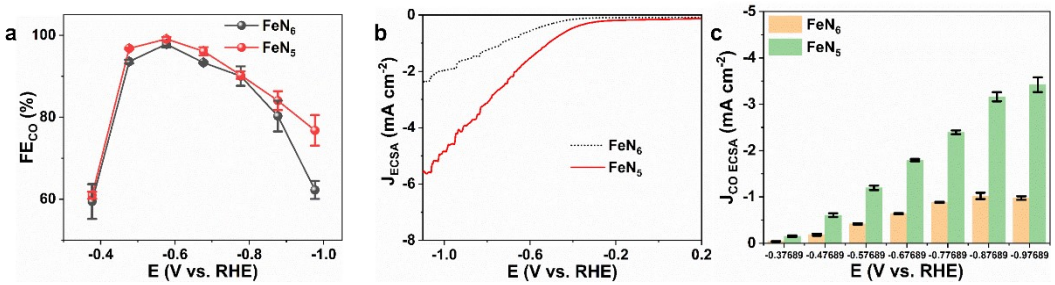

Figure S22. The performance comparison between FeN_5 and FeN_6 in 0.3 M $RbHCO_3$ (the current density is normalized by ECSA, Figure S20). (a) The FE_{CO}. (b) The LSV curves. (c) The J_{CO}.

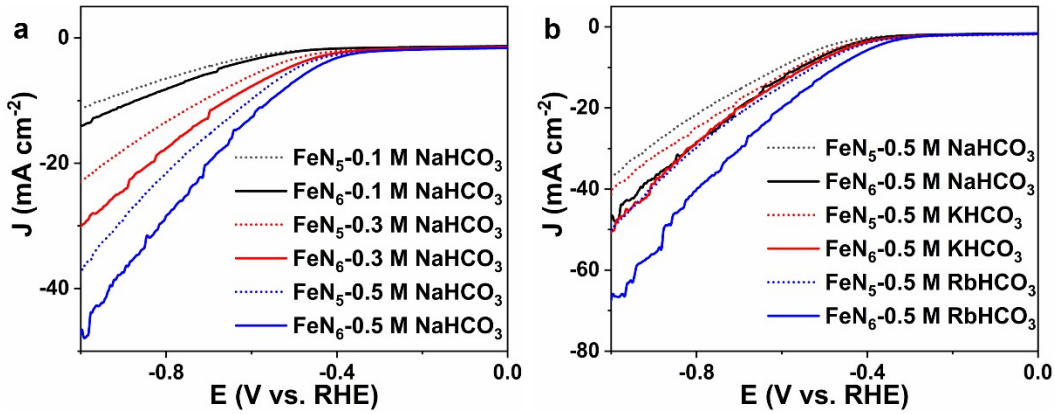

Figure S23. The LSV curves of FeN_5 and FeN_6 in Ar atmosphere with different electrolyte. (a) Different concentration. (b) Different cations.

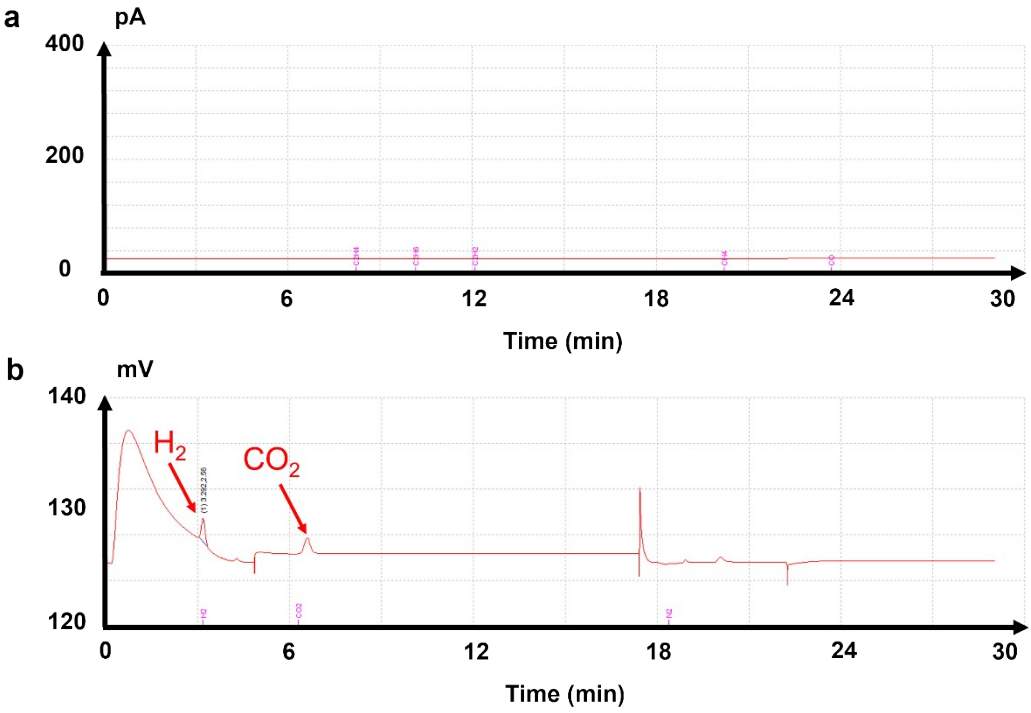

Figure S24. The GC of FeN_6 in Ar atmosphere (0.1 M $RbHCO_3$, -0.60 V vs. RHE). (a) The FID curve. (b) The TCD curve.

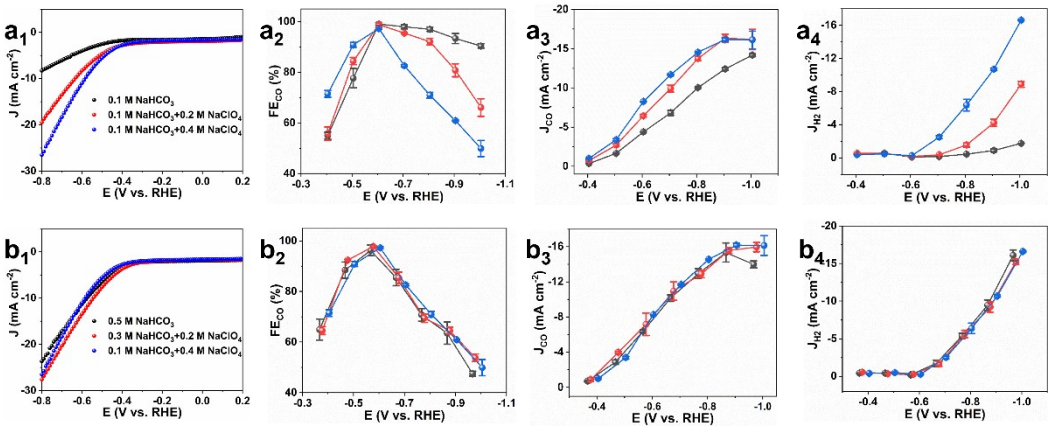

Figure S25. The CO_2 electroreduction performance of FeN_6 in constant cation and anion concentration. (a_1) The LSV, (a_2) FE_{CO}, (a_3) J_{CO} and (a_4) J_{H2} in constant concentration of HCO_3^-. (b_1) The LSV, (b_2) FE_{CO}, (b_3) J_{CO} and (b_4) J_{H2} in constant concentration of Na^+.

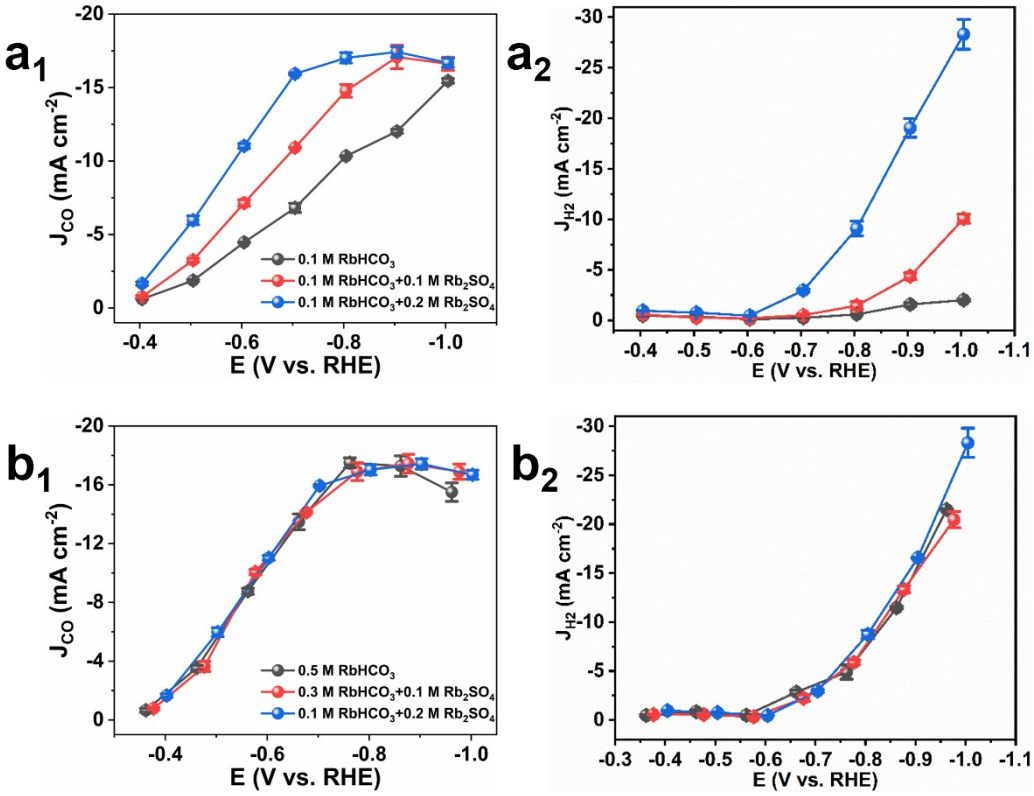

Figure S26. The CO_2 electroreduction performance of FeN_6 in constant cation and anion concentration. (a_1) J_{CO} and (a_2) J_{H2} in constant concentration of HCO_3^-. (b_1) J_{CO} and (b_2) J_{H2} in constant concentration of Rb^+.

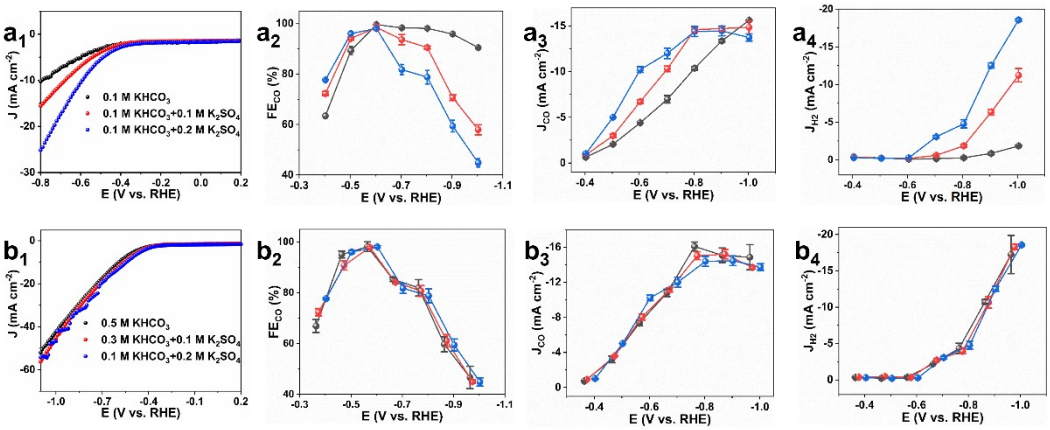

Figure S27. The CO_2 electroreduction performance of FeN_6 in constant cation and anion concentration. (a_1) The LSV, (a_2) FE_{CO}, (a_3) J_{CO} and (a_4) J_{H2} in constant concentration of HCO_3^-. (b_1) The LSV, (b_2) FE_{CO}, (b_3) J_{CO} and (b_4) J_{H2} in constant concentration of K^+.

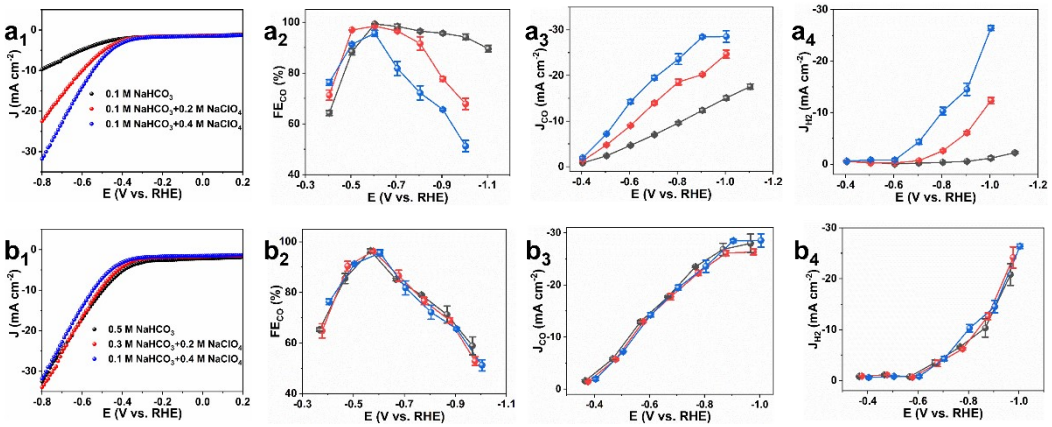

Figure S28. The CO_2 electroreduction performance of FeN_5 in constant cation and anion concentration. (a_1) The LSV, (a_2) FE_{CO}, (a_3) J_{CO} and (a_4) J_{H2} in constant concentration of HCO_3^-. (b_1) The LSV, (b_2) FE_{CO}, (b_3) J_{CO} and (b_4) J_{H2} in constant concentration of Na^+.

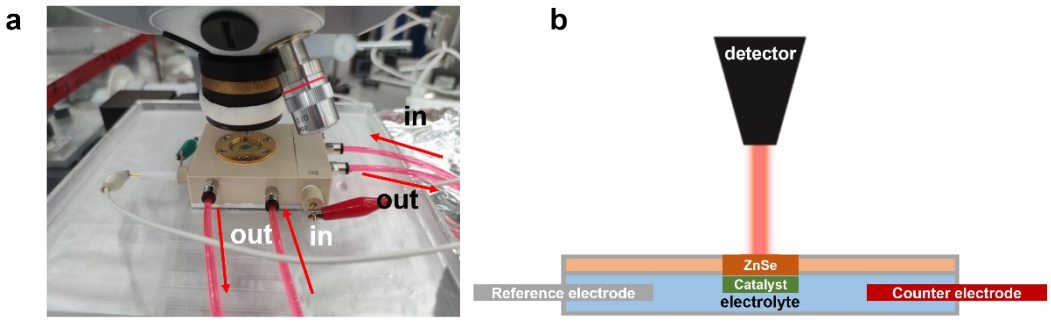

Figure S29. (a) The experimental setup for *in situ* SR-FTIR measurement. (b) The schematic of electrochemical cell for *in situ* SR-FTIR measurement.

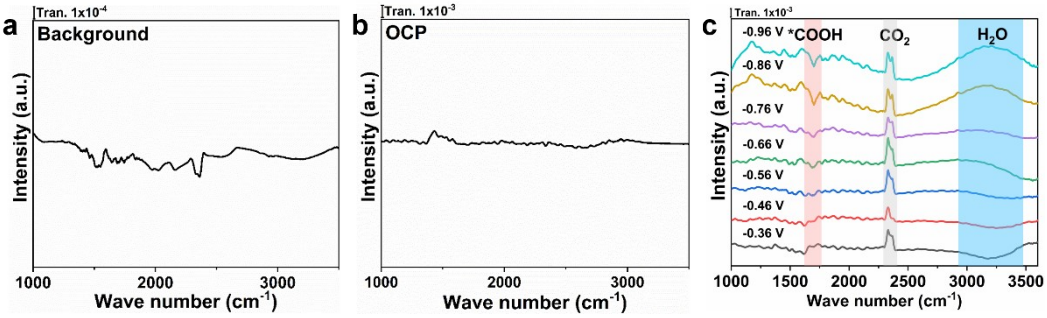

Figure S30. The *in-situ* SR-FTIR spectrum of FeN_6. (a) The background spectrum. (b) The OCP spectrum. (c) The spectrum at different potential (0.5 M $NaHCO_3$). The peak around 1700 cm^{-1}, 2360 cm^{-1} and 3150 cm^{-1} belong to *COOH, CO_2 and H_2O respectively, * denotes the adsorption site.[1-2]

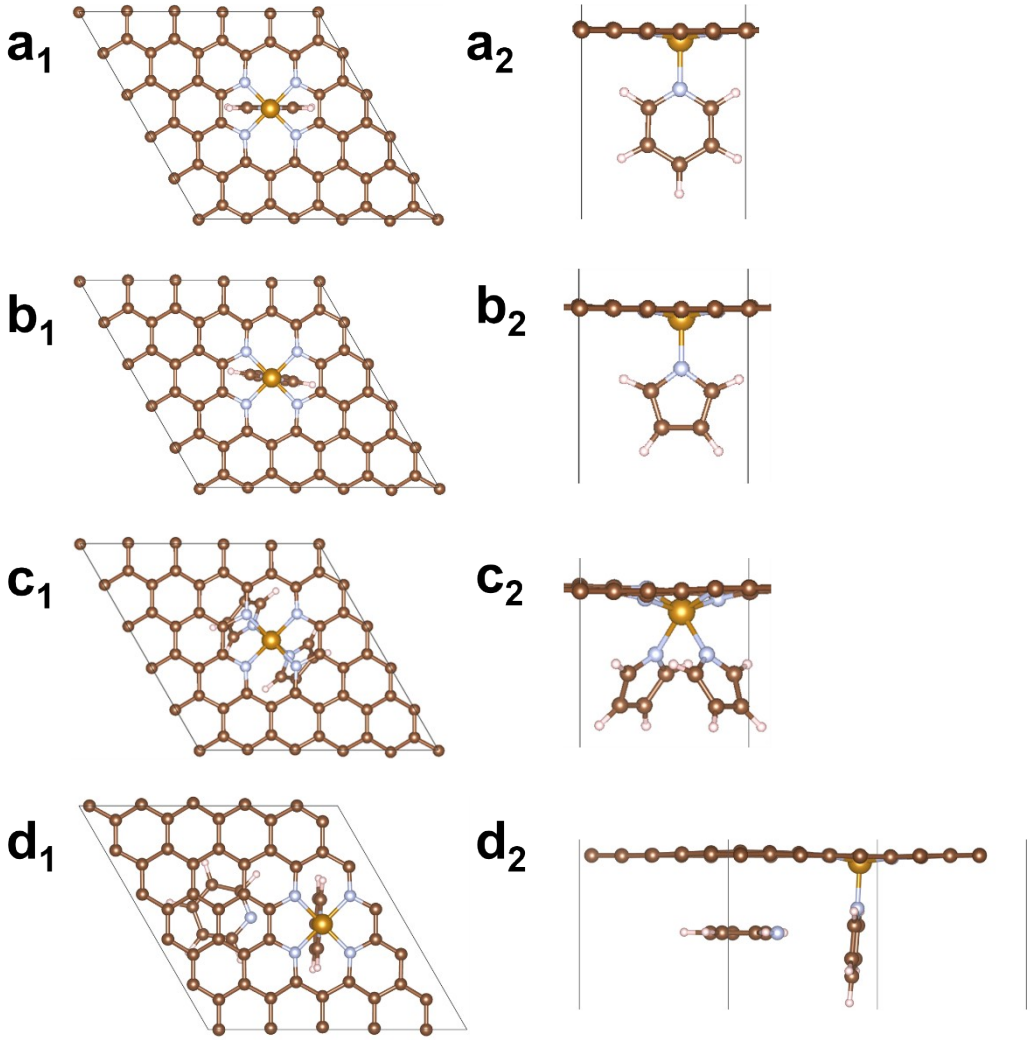

Figure S31. The top and side view of (a_1)-(a_2) FeN_5 (FeN_4 + pyridinic N), (b_1)-(b_2) FeN_5 (FeN_4 + pyrrolic N), (c_1)-(c_2) FeN_6 (FeN_4 + double pyrrolic N), (d_1)-(d_2) FeN_6 (FeN_4 + double pyridinic N).

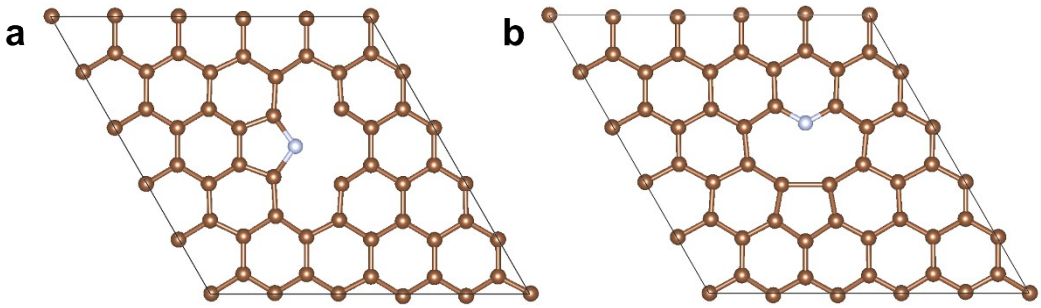

Figure S32. The top view of (a) pyrrolic N and (b) pyridinic N.

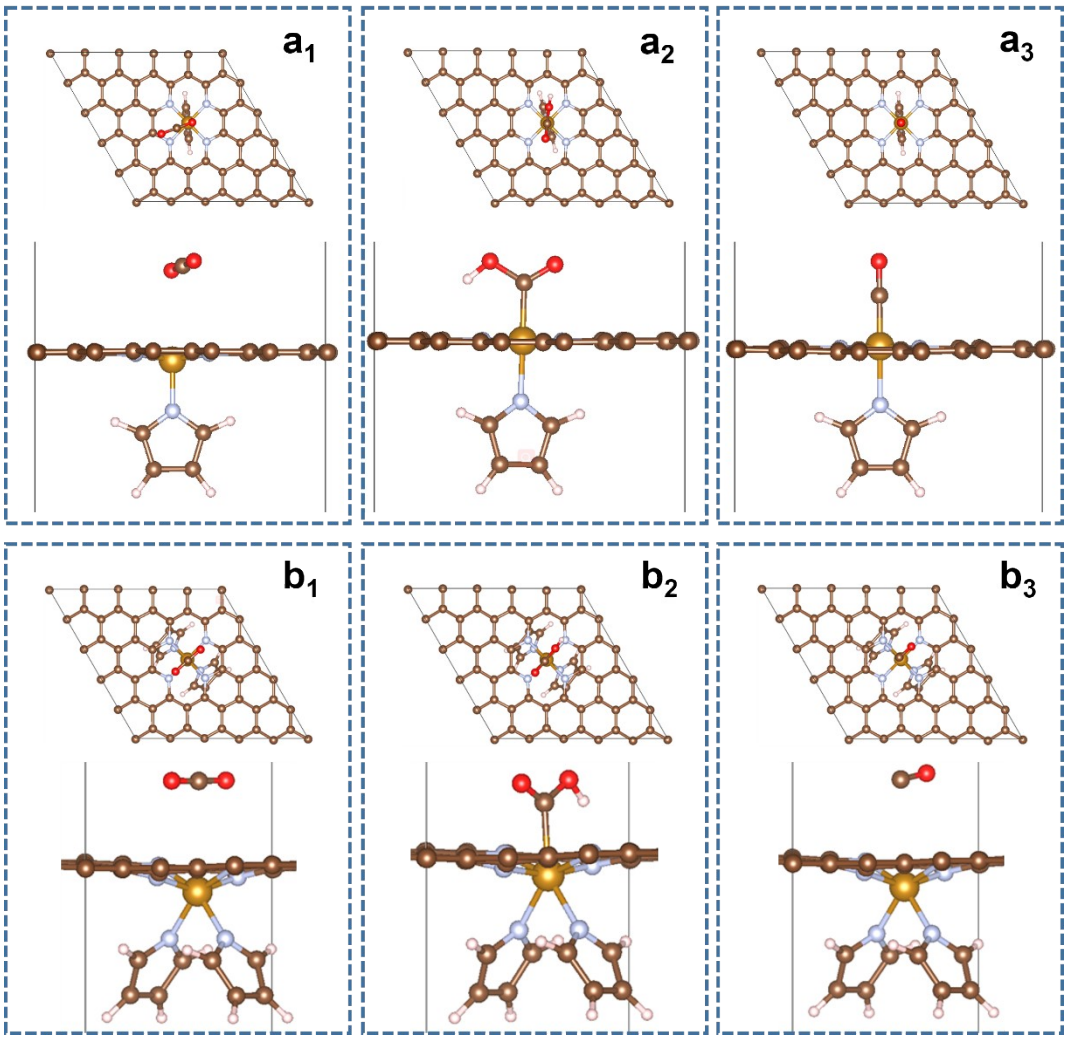

Figure S33. Optimized structures of FeN_5 and FeN_6 with adsorbed (a_1 , b_1) *CO_2, (a_2 , b_2) *COOH, (a_3 , b_3) *CO.

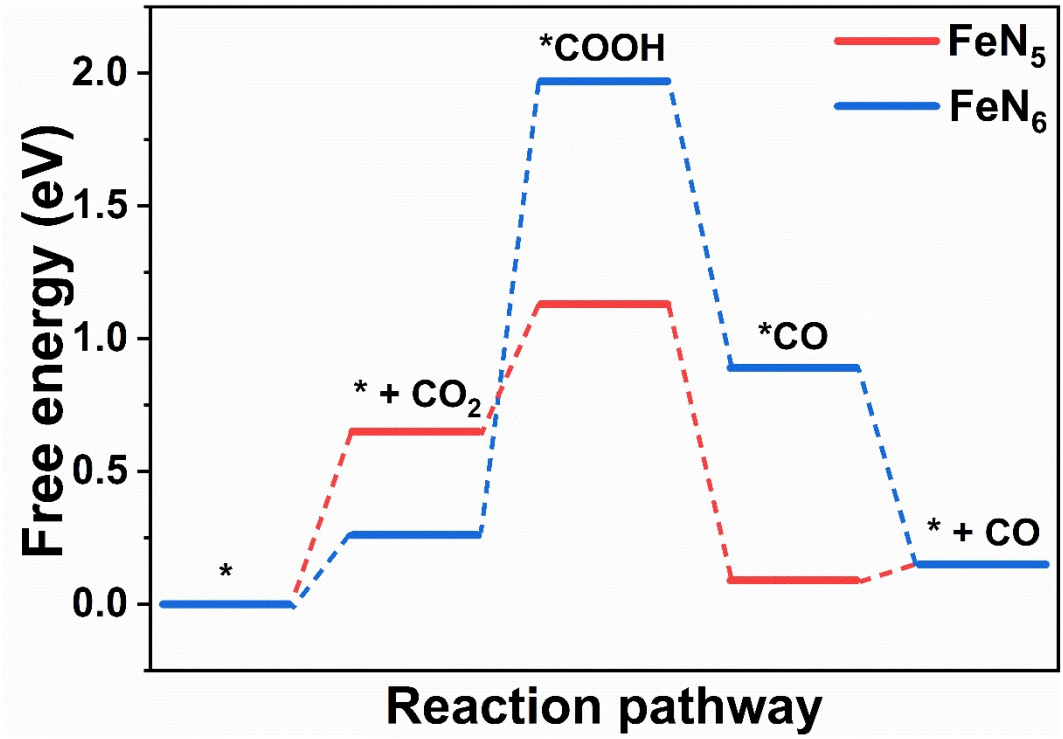

Figure S34. Calculated Gibbs free energy diagrams for CO_2 electroreduction to CO over FeN_5 and FeN_6 (vacuum condition).

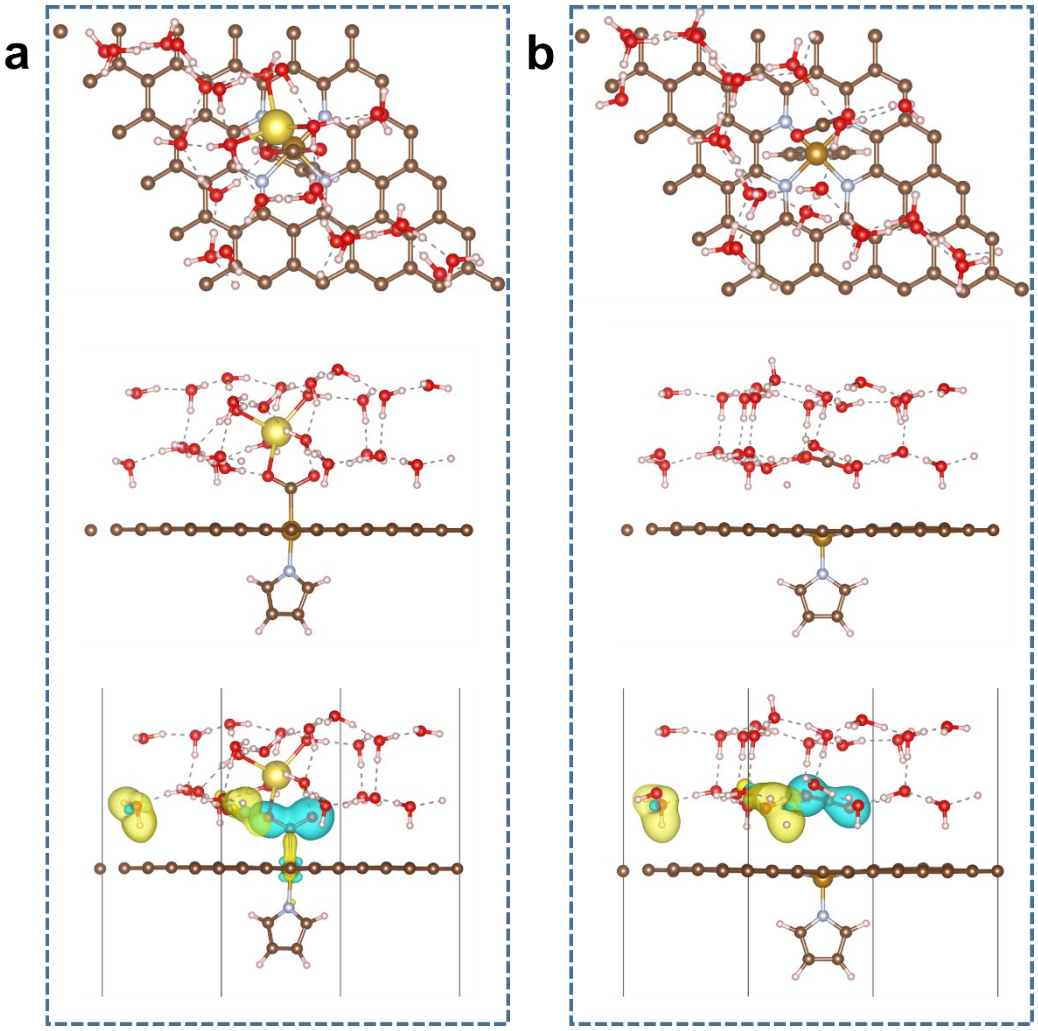

Figure S35. The top, side and charge density difference view of FeN_5 with adsorbed *CO_2 in different condition. (a) Na^+ and (b) pure water.

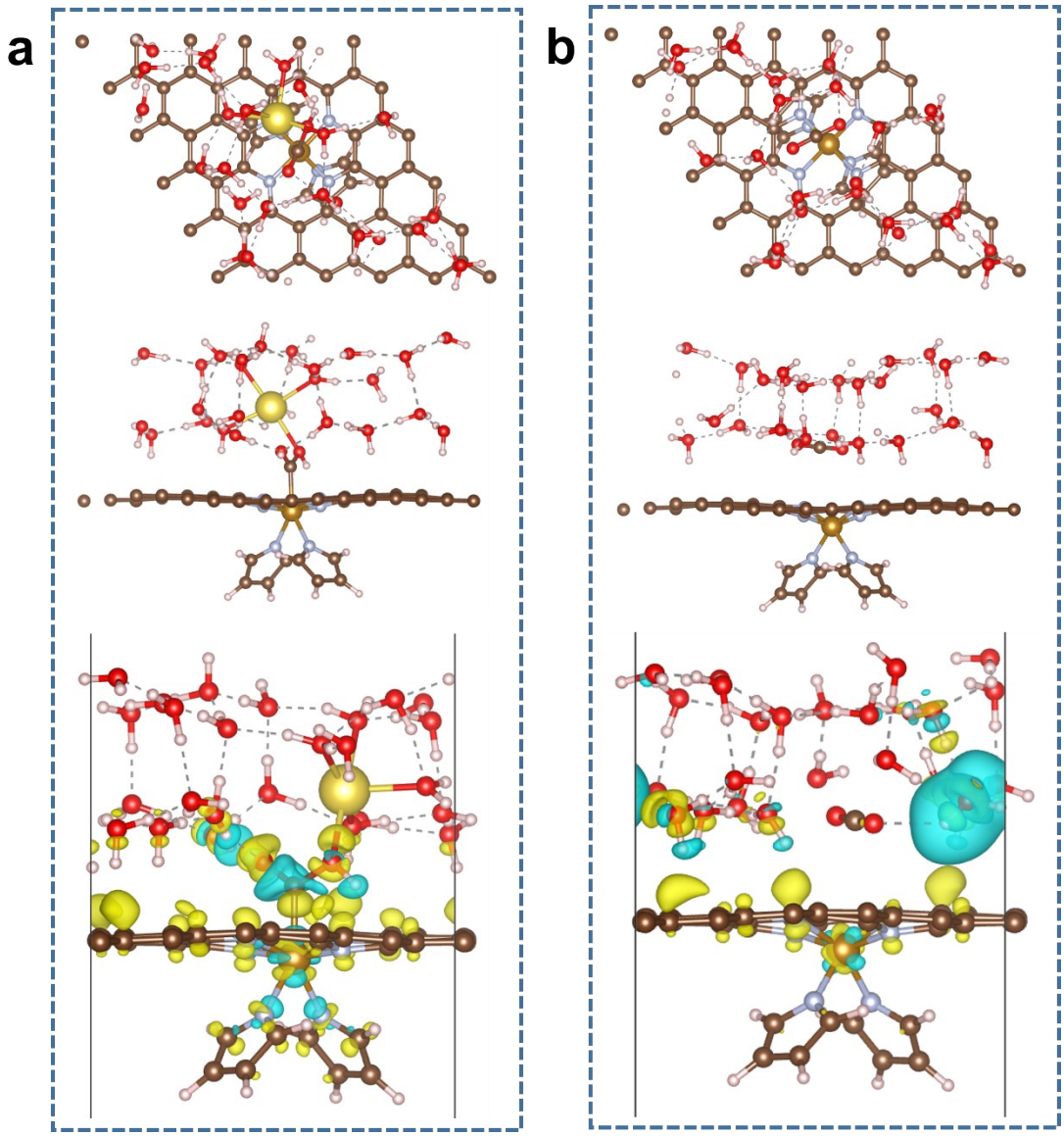

Figure S36. The top, side and charge density difference view of FeN_6 with adsorbed *COOH in different condition. (a) Na^+ and (b) pure water.

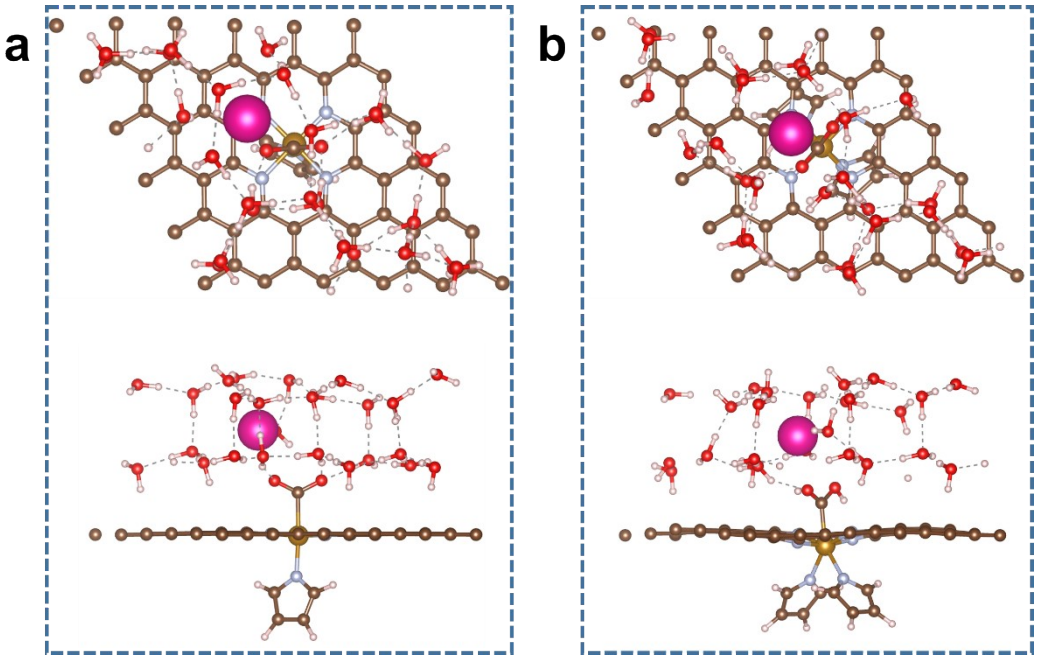

Figure S37. The top and side view of (a) FeN_5 with adsorbed $*CO_2$ in Rb^+ and (b) FeN_6 with adsorbed *COOH in Rb^+.

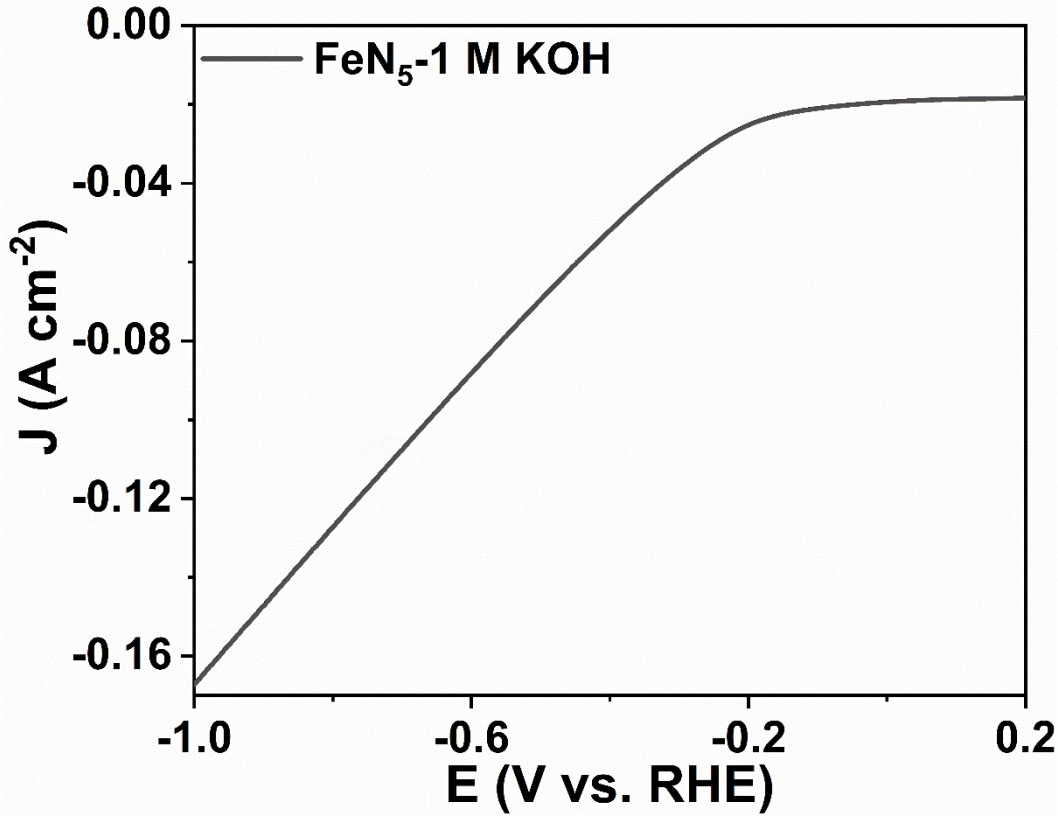

Figure S38. The LSV curve of FeN_5 under flow cell condition, 1 M KOH.

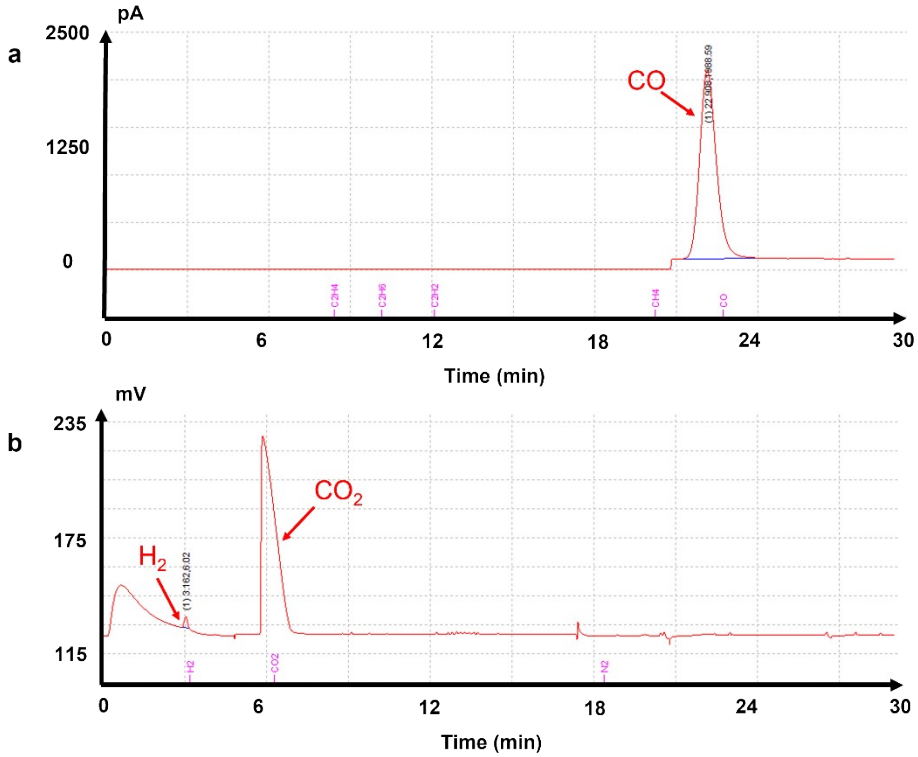

Figure S39. The GC of FeN_5 in CO_2 atmosphere (1 M NaOH, 100 mA cm^{-2}). (a) The FID curve. (b) The TCD curve.

Table S1. The BET results of different Fe SAC.

Sample	**FeN_6**	**FeN_5**
S_{BET} / m^2/g	766.5351	922.5563
Pore Volume / cm^3/g	1.837236	1.910247
Pore Size / nm	9.5872	8.2824

Table S2. The elements' content of different Fe SAC. The atom ratio and weight ratio were measured by XPS and ICP-AES respectively.

Sample	**FeN_6**	**FeN_5**
C (at%)	82.32%	88.57%
O (at%)	10.07%	4.72%
N (at%)	7.26%	6.22%
Fe (at%)	0.35%	0.49%
Fe (wt%)	1.90%	2.18%

Table S3. EXAFS fitting parameters at the Fe K-edge. (S_0^2=0.73)

Sample	Path	C.N.	R (Å)	$\sigma^2\times10^{-3}$ (Å^2)	ΔE (eV)	R factor
Fe foil	Fe-Fe	8*	2.47±0.01	4.9±1.6	-2.9±2.4	0.008
	Fe-Fe	6*	2.85±0.01	5.6±2.7	-3.3±3.8	
FeN_6	Fe-N/O	6.0±0.7	2.01±0.01	7.1±2.0	-0.6±1.1	0.018
FeN_5	Fe-N/O	5.5±0.5	2.01±0.01	7.3±1.6	-0.4±0.9	0.012

C.N.: coordination numbers; R: bond distance; σ^2: Debye-Waller factors; ΔE: the inner potential correction. R factor: goodness of fit. * Fitting with fixed parameter.

The obtained XAFS data was processed in Athena (version 0.9.26) for background, pre-edge line and post-edge line calibrations. Then Fourier transformed fitting was carried out in Artemis (version 0.9.26). The k^2 weighting, k-range of 3 – ~12 Å^{-1} and R range of 1 - ~3 Å were used for the fitting of standards; k-range of 2 – ~10 Å^{-1} and R range of 1 - ~3 Å were used for Fe samples. The four parameters, coordination number, bond length, Debye-Waller factor and E_0 shift (CN, R, σ^2, ΔE_0) were fitted without anyone was fixed, constrained, or correlated. For Wavelet Transform analysis, the χ(k) exported from Athena was imported into the Hama Fortran code. The parameters were listed as follow: R range, 1 - 4 Å, k range, 0 - 13 Å^{-1} for standards and 0 - 11 Å^{-1} for Fe samples; k weight, 2; and Morlet function with κ=10, σ=1 was used as the mother wavelet to provide the overall distribution.

Table S4. Different kinds of N content based on high-resolution N element XPS result.

Sample	**FeN_6**	**FeN_5**
Pyridinic N	33.82%	31.04%
Fe-N	6.61%	15.23%
Pyrrolic N	23.03%	4.49%
Graphitic N	28.56%	42.46%
Oxidized N	7.98%	7.09%

Table S5. Different valence of Fe content of Fe SAC (calculated from XPS).

Sample	**FeN_6**	**FeN_5**
Fe^{2+}	57.87%	63.35%
Fe^{3+}	42.13%	36.65%

Table S6. The pH of different electrolyte.

Electrolyte	Before saturate CO_2	After saturate CO_2	After saturate Ar
0.1 M $NaHCO_3$	8.28	6.62	None
0.1 M $KHCO_3$	8.77	6.65	None
0.05 M Rb_2CO_3	11.37	6.62	8.87
0.3 M $NaHCO_3$	8.11	7.08	None
0.3 M $KHCO_3$	8.46	7.15	None
0.15 M Rb_2CO_3	11.45	7.09	8.82
0.5 M $NaHCO_3$	8.00	7.26	None
0.5 M $KHCO_3$	8.37	7.31	None
0.25 M Rb_2CO_3	11.53	7.34	9.11

T=298K

Table S7. The pH of different electrolyte (constant HCO_3^- concentration, change Na^+ concentration).

$NaHCO_3$	$NaClO_4$	pH
0.1 M	0 M	6.62
0.1 M	0.2 M	6.62
0.1 M	0.4 M	6.62

Table S8. The pH of different electrolyte (constant Na^+ concentration, change HCO_3^- concentration).

$NaHCO_3$	$NaClO_4$	pH
0.5 M	0 M	7.26
0.3 M	0.2 M	7.15
0.1 M	0.4 M	6.62

Table S9. The pH of different electrolyte (constant HCO_3^- concentration, change K^+ concentration).

$KHCO_3$	K_2SO_4	pH
0.1 M	0 M	6.65
0.1 M	0.1 M	6.65
0.1 M	0.2 M	6.65

Table S10. The pH of different electrolyte (constant K^+ concentration, change HCO_3^- concentration).

$KHCO_3$	K_2SO_4	pH
0.5 M	0 M	7.31
0.3 M	0.1 M	7.15
0.1 M	0.2 M	6.65

Table S11. The pH of different electrolyte (constant HCO_3^- concentration, change Rb^+ concentration).

Rb_2CO_3	Rb_2SO_4	pH (after saturate CO_2)
0.05 M	0 M	6.62
0.05 M	0.1 M	6.62
0.05 M	0.2 M	6.62

Table S12. The pH of different electrolyte (constant Rb^+ concentration, change HCO_3^- concentration).

Rb_2CO_3	Rb_2SO_4	pH (after saturate CO_2)
0.25 M	0 M	7.34
0.15 M	0.1 M	7.09
0.05 M	0.2 M	6.62

Table S13. The formation energy of two different FeN_5 structure ($E_{for} = E_{total} - E_{sub} - E_{mol}$, the lower E_{for} represent the more stable structure).

FeN_5 configuration	**E_{for} (eV)**
FeN_4 + pyrrolic N	-2.10
FeN_4 + pyridinic N	-0.97

Table S14. The adsorption energy of $*CO_2$ adsorbed on FeN_5 and *COOH adsorbed on FeN_6 under different cation condition.

Solution condition	**FeN_5 - $*CO_2$**	**FeN_6 - *COOH**
Pure water	-16.72 eV	-19.73 eV
Na^+	-18.06 eV	-21.30 eV
Rb^+	-19.11 eV	-23.62 eV

Table S15. The bond length between H atom in H_2O and O atom in intermediates.

Intermediate	Na^+	Rb^+
FeN_5 - $*CO_2$	1.69 Å	1.82 Å
FeN_6 - *COOH	1.74 Å	1.90 Å

Reference

(1)Liu, X.-C.; Wei, C.; Wu, Y.; Fang, Y.; Li, W.-Q.; Ding, R.-R.; Wang, G.; Mu, Y. *ACS Catal.* **2021,** *11*, 14986-14994.

(2)Pei, J.; Wang, T.; Sui, R.; Zhang, X.; Zhou, D.; Qin, F.; Zhao, X.; Liu, Q.; Yan, W.; Dong, J.; Zheng, L.; Li, A.; Mao, J.; Zhu, W.; Chen, W.; Zhuang, Z. *Energy Environ. Sci.* **2021,** *14*, 3019-3028.